Influence of surface support properties on the liquid-phase selective hydrogenation of phenylacetylene on supported nickel catalysts

Felipa M. Bautista, Juan M. Campelo, Angel Garcia, Diego Luna *, José M. Marinas, Rafael A. Quiros and Antonio A. Romero

Department of Organic Chemistry, Sciences Faculty, University of Córdoba, Av. S. Alberto Magno, s/n°, E-14004 Cordoba, Spain

Received 27 October 1997; accepted 9 April 1998

The role of textural and acid–base properties of supports on metal–support interaction effects has been evaluated through the results obtained in the liquid-phase selective hydrogenation of phenylacetylene carried out on 20 wt% supported nickel catalysts. SiO_2, Al_2O_3, $AlPO_4$, active carbon and a natural sepiolite were used as supports. The effects of Ni–Cu alloying were also studied. The relative adsorption constants, $K_{T,D}$, and the relative reactivities, $R_{T,D}$, obtained in the consecutive hydrogenation process, were used to follow the effects of any electron transfer between the nickel atoms and acid–basic sites on the support surface. Structural defects of supported nickel crystallites were determined by X-ray diffraction line broadening analysis and used for measuring the participation of geometric effects of supported nickel crystallites in the catalytic activity. Results obtained may be better explained within a framework of simultaneous electronic and structural metal–support interaction effects.

Keywords: liquid-phase phenylacetylene hydrogenation, supported nickel catalysts, metal–support interaction effects, acid–base properties of supports, structural defects of crystallites

1. Introduction

Supported nickel catalysts are industrially important in methanation, hydrogenation and steam-reforming reactions, and, in this respect, the belief that the support component is merely an inert inorganic compound, used mainly to disperse the active metal component to prevent sintering and deactivation, is not valid since many years [1]. Thus, the subject of a great part of current research in catalysis by metals is strong metal–support interaction effects or SMSI. This refers to the inability of some supported metal particles to adsorb hydrogen and/or carbon monoxide after a reduction at temperatures where the support is known to be at least partially reduced [2–7]. This behavior, initially associated with reducible transition-metal oxides like TiO_2 [4–7], ZrO_2 [8–10] or Nb_2O_5 [11–13], has now been extended to "normal" supports like Al_2O [14,15] and SiO_2 [15,16] or some materials such as $AlPO_4$ [17–19]. However, the nature of the metal–support interactions in those conventional non-reducible supports seems to be different from that of classical metal-supported TiO_2 catalysts, where the reducibility of support is a key factor for the development of SMSI. The effect of SMSI on the catalytic activity and selectivity of different reactions is actually explained by the so-called "decoration model" [5,12,20,21], a geometric effect of metal surface coverage.

In the "normal" supports, it is still unclear why the support promotes important changes in the catalytic behavior, and several kinds of geometric (ensemble) effects as well as electronic (ligand) effects are shown to be important depending on the kind of metal and support [12,15]. Thus, since the first discovery made by Solymosi [22] and Schwab [23], many studies have demonstrated that change in the electron density of the metal, because of the transfer of electrons from support to metal or vice versa, can significantly modify chemisorption and catalytic properties [3,9,24–26]. However, other explanations for this behavior have been suggested, such as different morphological changes in the active metal [27]. Besides, suggestions have been made that any of the models alone cannot explain metal–support interaction effects in normal catalysts [28,29] and energetic, electronic and geometric properties of supported metal particles are simultaneously modified by electronic metal–support interaction and by changes from bulk to atom properties of the metal. Both effects become more important as the particle size of the metal becomes smaller, and it will not always be easy to distinguish between the relative contributions of electronic and structural or geometric effects on catalytic (and/or chemisorptive) properties of supported metal [30].

The existence of metal–support interactions effects on amorphous $AlPO_4$-supported nickel catalysts has been previously obtained on the kinetic behavior of catalysts [17–19,31–37], on suppression of hydrogen chemisorption [18,35], as is typical of SMSI oxide supports, by using a poisoning titration method [31] and on magnetic studies [38]. Besides, the results previously obtained in the liquid-phase hydrogenation of 1,4-butynediol [19] indicate that catalytic activity, selectivity and metal surface area of catalysts are closely correlated to some textural and/or acid–base properties of the corresponding support and that elec-

* To whom correspondence should be addressed.

tronic and geometric effects were simultaneously developed throughout metal–support interactions.

The present paper reports on research into the relative influence of geometric and electronic effects of some conventional non-reducible supports, including $AlPO_4$, on the catalytic behavior of supported nickel catalysts in the liquid-phase hydrogenation of phenylacetylene. The liquid-phase hydrogenation of higher alkynes, such as phenylacetylene, has been only lightly studied [39–42], however, from kinetic analysis of the consecutive hydrogenation, we can obtain $K_{T,D}$, the relative adsorption constant of the triple bond with respect to the double bond for different catalysts [19, 34,41,42]. These values, according to the results previously described for the competitive hydrogenation of toluene and benzene on several supported noble metals [43–45], including nickel supported catalysts [46–48], may be used to follow the changes in the electronic structure of supported nickel crystallites. Thus, $K_{T,D}$ values, as well as all the other kinetic parameters obtained in the liquid-phase consecutive hydrogenation of phenylacetylene, could be correlated with the support acid–base properties of the nickel supported catalyst, in order to test the electronic influence on metal–support interaction effects. Otherwise, some correlation between support textural properties and kinetic parameters could be related to geometric effects of the support on nickel particle size or nickel particle morphology.

The occurrence of electronic effects cannot be absolutely excluded because small metal particles in support cavities are clearly electron-deficient [49,50], due to some transfer of charge to neighboring highly acidic protons. Besides, the shape and crystallography of metallic particles seem to play an important role in the properties of supported metal catalyst [27,51–53]. Thus, in catalysis on single metal crystals, step or corner atoms show different catalytic properties than terrace atoms [52,53]. However, although there is evidence to suggest that crystal defects may provide active sites in supported metal catalysts, the exact nature and function of the sites is not yet well known. With regard to this, it was recently established that, in some catalytic reactions, not only metallic dispersion but also the microstructure of metal particles must be considered as factors controlling selectivity [54].

The peak shift of X-ray diffraction lines is a very important indicator of alteration in the metal microstructure. If there are no faults, the peak position is sufficient to describe the crystal and lattice parameters. If the concentration of faults is high, the structure peaks have to be displaced from their correct positions. Peak shifts can be caused by a change in the lattice parameters, by microstresses and by the presence of intrinsic and extrinsic stacking faults [55]. In other way, defects in the broad sense include different effects that should be evaluated separately. Thus, X-ray diffraction line broadening analysis (XRDLBA) has been extensively used to evaluate defect structures in metals, averaged to a significantly large volume sample [56–59]. The different measurements include the size of the coherent diffraction domains in selected crystallographic directions and the content in microstrains, as referred to the variations of interplanar spacing due to the presence of dislocations. Both parameters can be easily determined from the lorentzian and gaussian components of line breadth, respectively [60]. Further analysis of other effects, such as the asymmetric broadening of the profiles and, hence, a shift of the center of gravity of peaks, may provide information on the presence of twin faults [61]. A shift in the position of the XRD peak can also be used to identify the occurrence of stacking faults in the metal lattice [62].

In the present paper, structural defects of supported nickel crystallites are evaluated by an X-ray diffraction line broadening analysis (XRDLBA). These parameters will be correlated with textural and acid–base properties of supports in order to evaluate the potential correlation between the two kinds of parameters. Furthermore, the influence of former structural parameters on catalytic activity and selectivity in the liquid-phase hydrogenation of phenylacetylene will also be determined.

2. Experimental

2.1. Catalysts

Some catalysts used were previously described in the liquid-phase hydrogenation of 1,4-butynediol [19]. These catalysts, containing 20 wt% nickel, were prepared by impregnation of the supports to incipient wetness with 10 M aqueous nickel nitrate, following the procedure previously described [31–36,63–67]. They were dried, crushed and screened to particle size $<$0.149 mm (10 mesh size), reduced in an ultrapure hydrogen stream (1.7 $cm^3\,s^{-1}$) at 400 °C for 4 h, and then cooled to room temperature in the same hydrogen stream.

Amorphous $AlPO_4$ was obtained according to the sol–gel method previously described [19,31–36,68–72]. This support was prepared by precipitation from aqueous solutions of $AlCl_3{\cdot}6H_2O$ and H_3PO_4 (85 wt%) at pH = 6.1 at the "precipitation end-point", with ammonium hydroxide solution. The solid obtained was then washed with isopropyl alcohol and dried at 120 °C for 24 h. The resulting powder screened at 0.120–0.149 mm was calcined for 3 h in an electric muffle furnace at 650 °C. Furthermore, some habitual commercial materials such as a silica from Merck (Kieselgel 60, 70–230 mesh), SiO_2, an alumina (aluminum oxide active acidic for chromatography) from Merck, Al_2O_3, and an active carbon from Panreac, C, as well as natural sepiolite from Vallecas (Madrid), supplied by Tolsa S.A., Sep, were also used as the support, after undergoing the same calcination treatment. In addition, in order to evaluate the role of Cu in Ni–Cu alloying, three Ni–Cu bimetallic systems, containing 20 wt% Ni and 0.3 wt% Cu, were prepared using as supports $AlPO_4$, Sep and C. In these bimetallic catalysts, copper nitrate was also used in the impregnation step. Besides, four commercial nickel catalysts from Harshaw Chemie B.V. were used as

Table 1
Textural and acid–base properties of different supports.

Support	S_{BET} ($m^2\,g^{-1}$)	V ($ml\,g^{-1}$)	d (nm)	Acidity[a] vs. PY	Basicity[a] vs. BA
$AlPO_4$	156	0.68	3.6	190	200
Al_2O_3	72	0.24	2.7	23	191
SiO_2	366	0.68	3.5	206	164
C	743	0.55	1.5	124	132
Sep	203	0.54	5.3	31	174

[a] Values of the monolayer coverage at equilibrium in $\mu mol\,g^{-1}$.

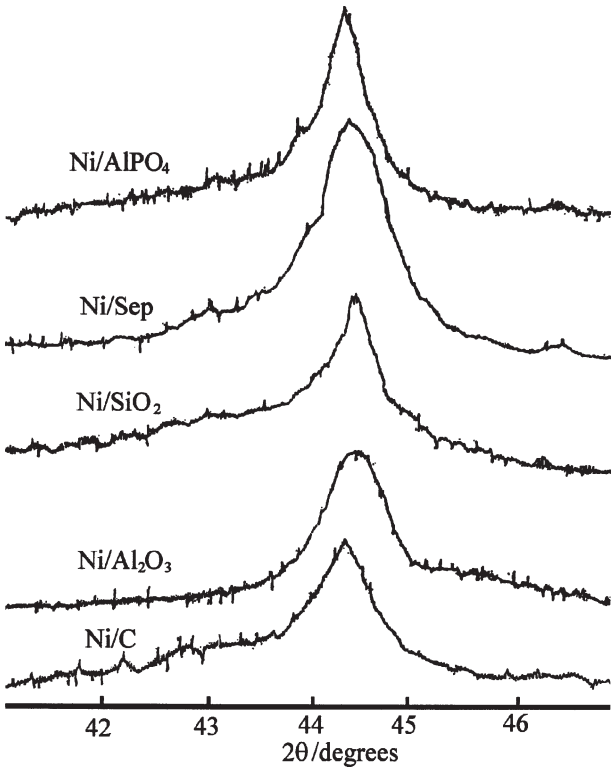

Figure 1. X-ray diffraction spectra of different supported nickel catalysts obtained after correction by the step scan technique.

references: a Ni-5333-T (20 wt% Ni), a Ni-5132-P (64 wt% Ni), a Ni-3210-T (35 wt% Ni) and a Ni-6458-T (60 wt% Ni).

Textural properties of supports (surface area, S_{BET}, pore volume, V, and main pore diameter, d) determined by nitrogen adsorption [36,73] are summarized in table 1, where the surface basicity and acidity are also collected. These values were determined by a spectrophotometric method, described elsewhere [74], that allows titration of the amount of irreversibly adsorbed benzoic acid (BA, $pK_a = 4.19$) or pyridine (PY, $pK_a = 5.25$) employed as titrant agents of basic and acid sites, respectively. The monolayer coverage at equilibrium at 25 °C, X_m (in $\mu mol\,g^{-1}$), is accomplished by applying the Langmuir adsorption isotherm, and is assumed as a measure of the acid or basic sites corresponding to the specific pK_a of the base or acid used as the titrant.

Table 2
Particle size, metal surface area and structural defects of nickel crystallites obtained from X-ray diffraction line broadening analysis of supported Ni and Ni–Cu catalysts.

Catalysts	$e \times 10^3$[a]	$[2\theta]_{111}$[b]	$2\theta_c - 2\theta_p$[c]	ε[d]	D[e]	S_{Ni}[f]
$Ni/AlPO_4$	4.27	44.40	0.34	78.5	150.2	44.9
Ni/Al_2O_3	6.66	44.47	0.02	53.5	107.4	62.8
Ni/SiO_2	8.11	44.58	0.42	53.7	113.8	59.2
Ni/C	0.91	44.40	0.34	89.5	110.5	61.0
Ni/Sep	3.89	44.40	0.16	94.9	91.7	73.5
Ni–Cu/C	1.34	44.40	0.32	79.5	92.9	72.6
Ni–Cu/$AlPO_4$	–[g]	–[g]	–[g]	–[g]	103.7	65.0
Ni–Cu/Sep	–[g]	–[g]	–[g]	–[g]	87.5	77.0

[a] Microstrains.
[b] Bragg angle in degrees used to identify "stacking faults" from peak position shifts.
[c] Twin faults in degrees from the shift of the center of gravity peaks.
[d] Crystallite diameter or domain size in nm determined from Pearson-VII function.
[e] Crystallite diameter in nm determined from Scherrer equation.
[f] Metal surface area from D, in $m^2\,g^{-1}$(Ni).
[g] Diffraction spectra obtained do not let apply Pearson-VII function to determine structural defects.

2.2. Characterization of the catalysts

X-ray powder diffraction analyses were recorded with a Siemens D500 diffractometer working with Cu K_α radiation monochromated by a graphite crystal. The data collection was performed with a DACO-MP system. The profiles for XRDLBA were recorded by the "step scan" technique with a step width of 0.02° 2θ. Background was automatically corrected by the DACO-MP system and α_2-elimination was carried out by the Rachinger method [75]. Results obtained for different catalysts are shown in figure 1. Bulk Ni powder was used as the standard for the correction of instrumental broadening, and Si powder for peak position, $[2\theta]_{111}$, measurements. Position shifts were used to identify the occurrence of stacking faults in the metal lattice [62]. Single-line broadening analysis was performed by profile fitting to Pearson-VII functions [76]. Crystallite size, ε, and microstrains, e, were computed from the Cauchy and Gauss components of the pure profile integral-breadths. These were deconvoluted from the full width at half maximum (FWHM) to integral breadth, β, ratio. The difference between peak and centroid position, $2\theta_c - 2\theta_p$, was also computed to evaluate the possible presence of twin-faults.

The metal surface area, S_{Ni}, of supported nickel catalysts was obtained from the average crystallite size diameter, D, determined by X-ray diffraction according to the method of Moss [77] by using the classical Scherrer equation [78], as has been described elsewhere [31–36]. Thus, the most common evaluation of crystallite size from FWHM was also carried out, assuming that the complete broadening was due to small crystallite effects. Table 2 summarizes the metal surface area, S_{Ni}, both average crystallite diameters, D and ε, as well as the corresponding structural parameters of supported catalysts.

Table 3
Catalytic activity and selectivity in the individual and consecutive hydrogenation of phenylacetylene and styrene on supported Ni and Ni–Cu catalysts under standard conditions.

Catalysts	r_T (μmol s^{-1} g^{-1})	r_D (μmol s^{-1} g^{-1})	S (%)	$R_{T,D}$	$K_{T,D}$
Ni/$AlPO_4$	9.33	140.2	88.6	9.10	136.74
Ni/Al_2O_3	19.83	145.9	89.7	13.27	97.60
Ni/SiO_2	32.71	174.8	85.9	9.35	49.97
Ni/C	28.28	144.4	86.9	9.78	49.94
Ni/Sep	18.31	132.8	86.7	9.55	69.25
Ni–Cu/C	46.84	229.2	86.0	9.85	48.18
Ni–Cu/$AlPO_4$	24.33	154.2	89.2	13.33	84.51
Ni–Cu/Sep	21.94	91.2	87.1	9.85	40.93
Ni-5333-T	44.66	234.6	89.4	13.50	67.60
Ni-3210-T	24.98	118.8	88.6	11.46	54.53
Ni-6458-T	72.00	326.2	89.3	14.46	65.52
Ni-5132-P	183.50	359.5	91.2	18.77	36.77

2.3. Hydrogenation reactions

According to the procedure previously employed [19, 31–36,67], hydrogenation runs were carried out in a closed vessel, under vigorous shaking (300 strokes min^{-1}) in a conventional low-pressure hydrogenator (Parr Instruments Co., model 3911) at controlled temperature conditions. The catalyst was always activated in an ultrapure hydrogen stream (1.7 cm^3 s^{-1}) at 400 °C for 1 h followed by cooling in the same hydrogen stream to room temperature. Afterwards, the activated catalyst was immediately added to the reaction vessel, containing 10 ml of 1 M methanolic substrate solution, in order to avoid reoxidation. The air in the vessel was removed by evacuation using a vacuum system until the solvent started to boil and the bottle with hydrogen to 0.27 MPa and venting it three times. The chromatographically pure phenylacetylene and styrene were used as supplied by Merck, p.a. after distillation under reduced pressure and low temperature. Methanol (p.a. 99%, Scharlau) employed as solvent and hydrogen (99.999%, SEO) was used without further purification.

Most hydrogenation reactions were carried out in 10 ml of 1 M methanolic substrate solution, at 40 ± 0.5 °C, under initial hydrogen pressure of 0.41 MPa, with 0.2 g catalyst. However, one set of reactions were carried out in the hydrogen pressure range of 0.3–0.7 MPa, temperature range 25–60 °C, a substrate concentration of 0.5–3 M and catalyst weight range 0.05–1.0 g in order to test the absence of transport influence in the kinetic data thus obtained. After purging the bottle, the hydrogen was introduced until the pressure reached the desired value. Then, agitation and timer were simultaneously started. The initial reaction rates in triple- and double-bond hydrogenation (r_T and r_D, respectively) were determined from a least-square fit to the initial slope of the plot of the hydrogen pressure decrease at the manometer versus time. Taking into account that the plots of the drop of the hydrogen pressure versus time were always practically linear until 80–90% conversion, the determination of the initial slope was straightforward. In the competitive reactions, there are clearly differentiated two

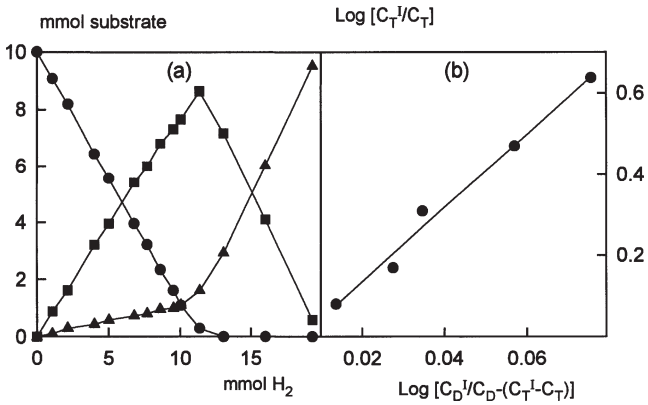

Figure 2. Consecutive hydrogenation of phenylacetylene on Ni/$AlPO_4$ catalyst under standard experimental conditions. (a) Distribution of reactant and products as a function of hydrogen consumption: (●) phenylacetylene, (■) styrene, (▲) ethylbenzene. (b) Logarithmic plot of the disappearance of phenylacetylene versus styrene according to equation (1).

parts, until 50% conversion, linear hydrogen pressure decrease at the manometer versus time was more slow than in the second part, indicating that reaction rates r_T are more slow than r_D, as can be seen in table 3. The consecutive hydrogenations were also followed by GLC with FID and a column packed with 5% Carbowax-20M in 80/100 Chromosorb GAW-DMCS, analyzing the reaction mixtures at appropriate intervals of hydrogen uptake (figure 2(a)). Neither isomerization nor hydrogenolysis products were detected in any of the cases.

3. Results and discussion

Several hydrogenation runs, performed at various agitation regimes and with different amounts of catalysts, showed the independence of the initial hydrogenation rate with respect to the agitation speed above 200 strokes min^{-1} and its linear variation with the catalyst loading, so that we can assume the absence of external diffusion control. The internal diffusion was excluded by using catalysts with a small enough grain diameter [79]. Experiments carried out under the same selected conditions with catalyst of several grain size showed that internal diffusion limiting the rate of hydrogenation is excluded when the grain size was lower than 0.21 mm [28–31]. The average particle size of the catalyst used (<0.149 mm) was such that the reactions were not influenced by internal diffusion. Thus, according to results previously obtained with other substrates [19,31–36,67], in this range of operating variables, the kinetic data obtained under the present experimental conditions are free from transport influences. The independence of the hydrogenation rate from the initial hydrogen pressure as well as from the concentration of both substrates, in the ranges studied, let us assume zero-order kinetics in hydrogen pressure as well as in substrate concentrations. This assumption is also consistent with the linear plots in the lowering of the hydrogen pressure versus time [80]. Thus, taking into account the zero-order kinetics obtained with respect to the

substrate concentration as well as to the hydrogen pressure, the initial reaction rates in triple- and double-bond hydrogenation (r_{T} and r_{D}, respectively) reported in table 3 can be used directly as the reaction constant values to obtain the relative adsorption constant of double bond with respect to triple bond for different catalysts, $K_{\mathrm{T,D}}$, by using the corresponding relative reactivity, $R_{\mathrm{T,D}}$, determined by introducing a modification [19,34,41,42,67] into the classical Rader–Smith kinetic equation [81] of competitive hydrogenations:

$$R_{\mathrm{T,D}} = \frac{r_{\mathrm{T}}}{r_{\mathrm{D}}} K_{\mathrm{T,D}} = \log\left(\frac{C_{\mathrm{T}}^{\mathrm{I}}}{C_{\mathrm{T}}}\right) \Big/ \log\left(\frac{C_{\mathrm{D}}^{\mathrm{I}}}{C_{\mathrm{D}} - (C_{\mathrm{T}}^{\mathrm{I}} - C_{\mathrm{T}})}\right), \quad (1)$$

where $C_{\mathrm{T}}^{\mathrm{I}}$ and $C_{\mathrm{D}}^{\mathrm{I}}$ are concentrations of T and D (phenylacetylene and styrene, respectively) when $C_{\mathrm{T}} = C_{\mathrm{D}}$. They are very easily obtained from the interception point of the distribution plots of the reactant and products in the course of the consecutive hydrogenation (figure 2(a)).

As you can see, equation (1) takes into account the additional concentration of D present in the reaction as a consequence of the consecutive transformation T → D, which may be evaluated as $C_{\mathrm{T}}^{\mathrm{I}} - C_{\mathrm{T}}$, when there are no secondary reactions, as obtained under the present experimental conditions. From the results of the consecutive hydrogenation shown in figure 2(a), we obtained the straight line shown in figure 2(b). The values of relative reactivity, $R_{\mathrm{T,D}}$, for all catalysts studied were determined from the slopes of the straight lines obtained in their log–log plots according to equation (1) and are shown in table 3, where $K_{\mathrm{T,D}}$ values are also summarized. On the other hand, the linearity of the plot in figure 2(b) can be taken as evidence of not only the validity of the theoretical treatment but also of the existence of a common (or very closely related) mechanism for double- and triple-bond hydrogenation reaction, within the framework of Langmuir–Hinshelwood kinetics [82–84].

Taking into account that relative reactivity, $R_{\mathrm{T,D}}$, is an index of the hydrogenation reactivity of alkyne compared to that of alkene, high values of $R_{\mathrm{T,D}}$ are consistent with the high selectivity, S, also shown in table 3, obtained from the relative concentration of alkene with respect to alkene and alkane at a very low concentration of alkyne [85]. Moreover, according to equation (1), $R_{\mathrm{T,D}}$ values are determined by two components, the ratio of the initial reaction rates $r_{\mathrm{T}}/r_{\mathrm{D}}$ and the relative adsorption constant values, $K_{\mathrm{T,D}}$. According to the results, the high values of $R_{\mathrm{T,D}}$, in spite of the low $r_{\mathrm{T}}/r_{\mathrm{D}}$ values are due to the high values of $K_{\mathrm{T,D}}$. Besides, the compensation between both parameters determines the very close $R_{\mathrm{T,D}}$ values obtained and, consequently, the narrow selectivity (86–91%) gap. Thus, high selectivity ought to be associated with the relatively high adsorptivity of the triple bond compared to that of the double one, owing to which the latter are hydrogenated only after all starting substrate has been taken up (figure 2(a)) [19,34,86].

In this respect, the relative adsorption constant of toluene with respect to benzene, $K_{\mathrm{T,B}}$, determined from a kinetic analysis of the competitive hydrogenation of these compounds, was used to probe the electronic structure of platinum and other group VIII metals [43,44,50]. Large $K_{\mathrm{T,B}}$ ratios were associated with the electron-deficient character of the metal. Thus, for a pair of hydrocarbons with different electronic structures, any change in the structure of the surface sites results in a modification of the relative adsorption constant value. In this respect, the modification of the electronic structure due to environmental effects (support acidity, electric field of cation adsorbates, or Pt–Zr bimetallic alloys) were monitored with a higher degree of sensitivity than that obtained by using physical techniques [43,87].

According to the results in table 3, all supports enhance the value of $K_{\mathrm{T,D}}$ to a variable degree with respect to the Ni/C, while $r_{\mathrm{T}}/r_{\mathrm{D}}$ exhibits the opposite behavior. In fact, there is a direct correlation between both kinetic data, as is shown in table 4, where are also collected the corresponding values of slopes and intercepts obtained in the regression analysis of those well-correlated parameter pairs obtained by developing a correlation matrix using all the data in tables 1, 2 and 3. Significance levels under 90% are not considered.

A direct correlation between the kinetic data, and the corresponding values of the acid–base properties of supports could indicate the existence of electronic metal–support interaction effects. The role of geometric effects of supports in determining the catalytic behavior of supported metal catalysts could be obtained from some correlation between kinetic data and structural defects of supported nickel crystallites.

According to these results, the compensation obtained between the two parameters $r_{\mathrm{T}}/r_{\mathrm{D}}$ and $K_{\mathrm{T,D}}$ can be explained from the relation obtained, in table 4, between both kinetic parameters and the surface basicity, BA, determined by titration with benzoic acid. Thus, according to the slopes (a values) in table 4, on increasing the number of surface basic sites, BA, there is an increase in $K_{\mathrm{T,D}}$ values and a decrease in the corresponding $r_{\mathrm{T}}/r_{\mathrm{D}}$ values. In the present case, on increasing the nucleophilic character of supports increased values of $K_{\mathrm{T,D}}$ are obtained. This behavior, associated with electronic nickel–support interaction effects, was also found in the consecutive hydrogenation of propargyl alcohols [34] and 1,4-butynediol [19]. Besides, the relative reactivity, $R_{\mathrm{T,D}}$, is also correlated with the surface density of basic sites, $\mathrm{BA}/S_{\mathrm{BET}}$, as well as with some textural properties of supports. Thus, low values of pore volume, V, and surface area, S_{BET}, promote and increase in $R_{\mathrm{T,D}}$ values. The correlations obtained between these textural properties and the number of acid and basic sites – PY vs. V, BA vs. S_{BET} and $\mathrm{BA}/S_{\mathrm{BET}}$ vs. $1/V$, all also collected in table 4 – indicate the complex influence of support surfaces on kinetic parameters.

All these facts could be explained within the framework of the prevailing role of an electronic transfer between sup-

Table 4
Regression coefficients from the correlation obtained between some surface properties of supports in table 1, some crystallite structure parameters in table 2, and the kinetic parameters of supported nickel catalysts in table 3, according to the general expression $y = ax + b$, as well as the corresponding significance levels.

y	x	a	b	Significance (%)
r_T/r_D	$K_{T,D}$	-1.3×10^{-3}	0.253	99.1
r_T/r_D	$1/K_{T,D}$	8.545	21.2×10^{-3}	98.5
r_T/r_D	BA	-1.7×10^{-3}	0.436	94.4
$K_{T,D}$	BA	1.188	−123.947	93.5
$R_{T,D}$	BA/S_{BET}	1.499	8.585	92.7
$R_{T,D}$	V	−9.267	15.196	99.2
$R_{T,D}$	$1/V$	1.512	6.951	100.0
$R_{T,D}$	$1/S_{BET}$	304.699	8.424	94.0
r_D/S_{Ni}	PY	5.5×10^{-3}	1.887	95.5
r_D/S_{Ni}	PY/S_{BET}	1.014	2.024	93.0
r_D	$[2\theta]_{111}$	192.419	−8405.420	98.5
r_D/S_{Ni}	D	0.021	0.081	94.1
$R_{T,D}$	$2\theta_c - 2\theta_p$	−8.775	12.456	91.6
$R_{T,D}$	$1/(2\theta_c - 2\theta_p)$	0.082	9.149	99.9
PY	V	393.936	−97.137	91.4
BA	S_{BET}	−0.095	201.443	98.7
BA/S_{BET}	$1/V$	0.738	−0.507	94.2
D	PY/S_{BET}	46.194	92.364	98.6
$1/e$	S_{BET}	1.37×10^{-6}	-49.5×10^{-6}	95.6
$1/e$	BA	-0.013×10^{-3}	2.539×10^{-3}	90.7
$1/e$	BA/S_{BET}	0.178×10^{-3}	0.011×10^{-3}	97.4
$1/e$	$1/d$	0.002	-0.339×10^{-3}	96.0
$2\theta_c - 2\theta_p$	V	0.823	−0.187	96.8
$1/(2\theta_c - 2\theta_p)$	$1/S_{BET}$	3929.711	−10.128	97.5
$1/(2\theta_c - 2\theta_p)$	BA/S_{BET}	19.445	−8.166	96.7
$2\theta_c - 2\theta_p$	PY	1.8×10^{-3}	0.055	97.6
$2\theta_c - 2\theta_p$	1/PY	−8.917	0.424	99.7

port and metal in determining the metal–support interaction effects. Thus, according to Bartholomew et al. [88], an electron transfer between the basic sites on the support and nickel atoms increases the d-band concentration of electrons in the metal crystallites leading to a catalytic behavior more characteristic of copper. So, the electrophilic character of nickel surface active sites will decrease and, consequently, the adsorption strength of both alkyne and alkene bonds as well as their hydrogenation rates will also decrease. In table 3, we can see that catalysts with the lowest $K_{T,D}$, such as Ni/SiO_2, Ni/C or Ni-5132-P, exhibit the highest catalytic activity in both r_T and r_D values as well as the opposite: higher $K_{T,D}$ values are associated to lower values of r_T and r_D, such as for $Ni/AlPO_4$or Ni/Al_2O_3.

Furthermore, taking into account that the nucleophilic character of an alkyne bond is higher than that of the alkene one, on decreasing the electrophilic character of nickel surface active sites, selectivity in the competitive adsorption of former molecules will increase with respect to latter ones. Thus, the highest values in $K_{T,D}$ could be obtained when (due to the higher number of basic sites in the support) the so much lower electrophilic character of nickel surface atoms does not allow the adsorption of the competing alkene molecules, which exhibit a lower nucleophilic character than the alkyne ones. Besides, the correlation obtained between the catalytic activity per unit metal surface area, or specific catalytic activity of styrene, r_D/S_{Ni}, and the surface density of acid sites of supports, PY/S_{BET}, can also be explained by the lower nucleophilic character of alkene what let it detect the differences in the electrophilic character of nickel surface active sites associated to the acidity of different supports. The nucleophilic character of an alkyne bond is high enough to erase the differences in the electrophilic character of nickel surface atoms due to the nickel–support interaction effects.

The influence of copper alloying may also be explained within the framework of the prevailing role of an electronic transfer between Cu and Ni in determining the catalytic behavior of bimetallic Ni–Cu supported catalysts. Thus, in table 3, we can see that on the three supports studied there is a variable increase in the quotient r_T/r_D associated to a decrease on $R_{T,D}$ values, on going from the Ni supported catalyst to the corresponding bimetallic Ni–Cu supported one. These changes in r_T/r_D and $R_{T,D}$ values, in the three bimetallic Ni–Cu catalysts studied, are similar to that obtained on going from Ni/C to more basic supports, so that they can be a consequence of the increased electronic density of the Ni d-band, which may be ascribed to an electronic transfer from Cu to Ni, with a variable contribution of the support, according to its electronic conduction properties. The inertness of the carbon preventing strong metal–support interactions [89] may explain the very low changes obtained in r_T/r_D and $R_{T,D}$ when this material is used as support, as compared to $AlPO_4$ and sepiolite.

Consequently, results obtained in the kinetic behavior of supported nickel catalysts indicate that some support effects, as well as the effects of Ni–Cu alloying, may be explained by using simple MO arguments, as a donor–acceptor interaction between the frontier orbital, π, of alkene or alkyne and the LUMO of surface nickel atoms [34,43].

However, the existence of electronic effects does not exclude the simultaneous presence of geometric effects of nickel crystallites on the catalytic hydrogenation process. Thus, according to the results in table 4, we can see the existence of some correlations between kinetic parameters, such as the relative reactivity, $R_{\mathrm{T,D}}$, or r_{D}, and parameters closely related to structural defects of supported nickel crystallites, such as twin faults, $2\theta_{\mathrm{c}} - 2\theta_{\mathrm{p}}$, or stacking faults, $[2\theta]_{111}$. Besides, the influence nickel particle size on the catalytic activity is also obtained through the correlation between the catalytic activity per unit metal surface area, or specific catalytic activity, $r_{\mathrm{D}}/S_{\mathrm{Ni}}$, and crystallite diameter, D.

In this respect, the origin of crystallite structural defects may be obtained from textural and acid–base properties of supports, according to the corresponding correlations also obtained between crystallite microstrains, e, and the support surface area, S_{BET}, pore diameter, d, and surface density of the basic sites of supports, $\mathrm{BA}/S_{\mathrm{BET}}$, as well as between crystallite twin faults, $2\theta_{\mathrm{c}} - 2\theta_{\mathrm{p}}$, and the S_{BET}, pore volume, V, surface density of the basic sites of supports, $\mathrm{BA}/S_{\mathrm{BET}}$, and surface acidity of supports, PY. A close relationship between surface density of the acid sites of supports, $\mathrm{PY}/S_{\mathrm{BET}}$, and nickel crystallite size, D, was also obtained.

It is worth noting that support surface area, S_{BET}, significantly affects crystal perfection of the supported metal particles. Thus, a high S_{BET} conditions an enhanced asymmetry of the profiles that can be related to the presence of antiphase domains in the metal particles, as stated in previous literature [61]. In contrast, high S_{BET} values imply a low content in microstrains. This, in turn, implies that the extensive twinning relaxes the internal strains in the [111] direction of the metal lattice. An increased number of basic sites seems to promote the perfection of supported nickel microstructure. By opposite, a high number of surface acid sites promotes not only an increase in the nickel supported particle size but also an increase in the concentration of defects in metal lattice parameters such as microstrains and twin faults.

In summary, on going from textural and acid–base properties of a support to the catalytic behavior of the corresponding Ni (or a bimetallic Ni–Cu) supported catalyst, we have that, according to the results obtained, textural properties alone are able to affect some crystallite defects such as twin faults or microstrains. Thus, high S_{BET} promote low microstrains and high levels in twin faults. Besides, acid–base properties promote changes at two levels, on structural defects as well as on the electronic density in Ni d-band. Thus, surface density of acid sites, $\mathrm{PY}/S_{\mathrm{BET}}$, is able to affect nickel particle size, D, twin faults, and specific catalytic activity, $r_{\mathrm{D}}/S_{\mathrm{Ni}}$. An increase in the surface density of basic sites, $\mathrm{BA}/S_{\mathrm{BET}}$, promotes a variable decrease in crystallite defects such as twin faults and microstrains, as well as higher values of $K_{\mathrm{T,D}}$, that can be associated to an increase of the electronic density of supported Ni atoms.

It is also conceivable that styrene hydrogenation can be a structure-insensitive reaction, according to Boudart [90], instead of the relationship obtained between particle size, D, and catalytic activity $r_{\mathrm{D}}/S_{\mathrm{Ni}}$. Thus, the correlation obtained between the specific number of acid sites, $\mathrm{PY}/S_{\mathrm{BET}}$, and the specific catalytic activity of styrene hydrogenation, $r_{\mathrm{D}}/S_{\mathrm{Ni}}$, as well as between the former and the nickel particle size, D, may give, as an artifact, the existence of the correlation between D and $r_{\mathrm{D}}/S_{\mathrm{Ni}}$. In this connection, it is possible that some other correlations shown in table 4 could be artifacts, obtained as a consequence of the correlations between some textural and acid–base properties of supports. However, on the basis of the present results, we may assume that textural and acid–base properties of supports play an important role in determining metal–support interaction effects not only by effects of an electron transfer between crystallite nickel atoms and acid–basic sites on the support surface, but also by their simultaneous action in determining in a variable extension different structural defects on nickel crystallites, probably at the end responsible for the concentration of active sites on the metal surface, where the liquid-phase catalytic hydrogenation is carried out [54].

Crystallite defects probably act on kinetic parameters through the specific number of active sites on the surface of nickel particles, n_{S} (number of active sites per unit surface area), while the final electronic level of nickel crystallites do it through changing the "turnover frequency", TOF (the rate of the reaction expressed in moles per exposed metal atom and per unit time). The "crystal defects" here considered may be the same as described by Somorjai [52,53] as steps, terraces and kinks, which set up the surface density of metal active sites. However, aside from n_{S} values, different electronic levels in Ni d orbital produce different TOF values. Thus, specific catalytic activity ($r_{\mathrm{T}}/S_{\mathrm{Ni}}$ and $r_{\mathrm{D}}/S_{\mathrm{Ni}}$) obtained from the product of the two parameters ($n_{\mathrm{S}} \times$TOF) ought to be necessarily related to both electronic and geometric crystallite parameters. The differences obtained between r_{T} and r_{D} in every catalyst could be due to the existence of different TOF values for different nickel supported (or Ni–Cu alloy supported) catalysts, associated with varying electronic metal–support interaction effects, taking into account that n_{S} is the same for every catalyst, due to the hydrogenation reaction mechanism of alkyne and alkene, consecutively carried out on the same active sites. Differences obtained in selectivity and catalytic activity of commercial catalyst may be ascribed in an important part to the differences in nickel loadings. With the exception of Ni-3210-T, increases in nickel loadings are associated to the highest values in selectivity and catalytic activity. These effects of nickel loading on catalytic activity and selectivity are not difficult to explain within the framework of a simultaneous action of electronic and structural or geometric effects on metal–support interaction effects.

4. Conclusions

Independent of the SMSI mechanism developed with TiO_2 and other reducible supports, where the participation of different coverage models or "decorations" would be possible [5,12], according to the present results the kinetic behavior of nickel catalysts supported on non-reducible supports may be explained by the simultaneous participation of electronic and structural effects in metal–support interaction.

On the other hand, based on these results and according to previous works [19,34], we may conclude that the modification introduced into the classical Rader–Smith equation [81] allows us to obtain $R_{T,D}$ and $K_{T,D}$ values in consecutive processes, such as the selective hydrogenation of alkynes, within the framework of Langmuir–Hinshelwood kinetics. These kinetic parameters can give us valuable information, not only concerning the hydrogenation mechanism of double and triple bond, but also on the parameters affecting the selectivity of the process as well as the electronic level of supported nickel, which is modified by support effect, metal/support ratio or Ni–Cu alloying. An increase in electronic density in Ni d-band promotes a variable increase in $K_{T,D}$, so that this kinetic parameter is a useful test in evaluating the existence of electronic metal–support interaction effects. The inconsistencies obtained by Vannice [45] on determining $K_{T,B}$ values in the gas-phase competitive hydrogenation of toluene and benzene are absolutely avoided when the consecutive (or competitive) reaction is carried out in liquid-phase, such as in the present case, because of under these soft conditions the possibility of secondary reaction products are absolutely excluded.

Results obtained by using Pearson-VII functions in the X-ray diffraction line broadening analysis to evaluate structural defects in supported nickel crystallites indicate that it may constitute an adequate technique for measuring the existence, extent and participation of geometric support effects in the catalytic activity of supported nickel catalysts. However, in this respect, while structural defects in metal crystallites promotes a notable influence in catalytic activity and selectivity, their contribution to the line broadening is less important so that the classical Scherrer equation actually constitutes an adequate technique for measuring average crystallite size diameters.

Correlations obtained between kinetic data, structural defects of supported nickel crystallites and textural and acid–base properties of supports indicated that electronic and geometric effects of nickel crystallites determined by the textural and acid–base properties of supports simultaneously act on the catalytic behavior of Ni supported catalysts. Thus, we can see how textural and acid–base properties act not only on particle size and structural defects of crystallites such as microstrains and twin faults, but also on $K_{T,D}$ [43,44,50,87], a kinetic parameter directly related to the electronic level of nickel surface active sites. Ni–Cu alloying also affects both kinds of parameters, those related to electronic effects, as well as those related to structural defects. Thus, the final electronic level of supported metal crystallites determining the "turnover frequency", TOF, as well as the specific number of surface-active sites of nickel particles, n_S, are determined by both textural and acid sites of the support, so that metal–support interaction effects, as well as Ni–Cu alloying, are explained within the framework of the simultaneous action of electronic and structural or geometric metal–support interaction effects.

Finally, taking into account that Ni–Cu alloy, in 20/0.3 wt% proportion, exhibits substantially higher catalytic activity than monometallic supported nickel catalysts, without loss in selectivity, Ni–Cu alloying could be an adequate procedure to enable tailored Ni–Cu supported catalysts, for the best selective liquid-phase hydrogenation of any alkyne, by using the most adequate nickel/support ratio and Ni–Cu proportion for a given conventional support.

Acknowledgement

This work was subsidized by the Dirección General de Investigación Científica y Técnica (DGICYT, project PB92-0816), Ministerio de Educación y Ciencia, as well as by the Consejería de Educación y Ciencia de la Junta de Andalucía. The authors would also like to thank Harshaw Chemie B.V. for providing some catalysts samples. The valuable help of Professor M. Sullivan in the grammatical revision of the manuscript is also acknowledged.

References

[1] A. Nielsen, Catal. Rev. Sci. Eng. 23 (1981) 17.
[2] S.J. Tauster, S.C. Fung and R.L. Garten, J. Am. Chem. Soc. 100 (1978) 170.
[3] S.J. Tauster, S.C. Fung, R.T.K. Baker and J.A. Horsley, Science 211 (1981) 1121.
[4] S.J. Tauster, Acc. Chem. Res. 20 (1987) 389.
[5] G.L. Haller and D.E. Resasco, Adv. Catal. 36 (1989) 173.
[6] J.P. Belzunegui, J. Sanz and J.M. Rojo, J. Am. Chem. Soc. 114 (1992) 6749.
[7] A.C. Faro, Jr. and C. Kemball, J. Chem. Soc. Faraday Trans. 91 (1995) 741.
[8] P.D.L. Mercera, J.G. van Ommen, E.B.M. Doesburg, A.J. Burgraaf and J.R.H. Ross, Appl. Catal. 57 (1990) 127.
[9] H. Yoshitake and Y. Iwazawa, J. Phys. Chem. 96 (1992) 1329.
[10] B. Coq, P.S. Kumbhar, C. Moreau, P. Moreau and F. Figueras, J. Phys. Chem. 98 (1994) 10180.
[11] E.I. Ko, R. Bafrali, N.T. Nuhfer and N.J. Wagner, J. Catal. 95 (1985) 260.
[12] T. Uchijima, Catal. Today 28 (1996) 105.
[13] R. Brown and C. Kemball, J. Chem. Soc. Faraday Trans. 92 (1996) 281.
[14] T.C. Chang, J.J. Chen and C.T. Yeh, J. Catal. 96 (1985) 51.
[15] S. Narayanan and G. Sreekanth, J. Chem. Soc. Faraday Trans. 85 (1989) 3785.
[16] R. Lamber, W. Jaeger and G. Schulz-Ekloff, J. Catal. 123 (1990) 285.
[17] J.M. Campelo, A. Garcia, D. Luna and J.M. Marinas, Appl. Catal. 3 (1982) 315.
[18] G. Marcelin, R.F. Vogel and H.E. Swift, J. Catal. 83 (1983) 42.
[19] J.M. Campelo, R. Guardeño, D. Luna, J.M. Marinas, J. Morales and J.L. Tirado, J. Mol. Catal. 85 (1993) 305.

[20] G.C. Bond, R.R. Rajaram and R. Burch, in: *Proceedings 9th International Congress Catalysis*, Vol. 3, eds. M.J. Phillips and M. Ternan (Chem. Inst. Canada, Ottawa, 1988) p. 1130.
[21] S. Bernal, F.J. Botana, J.J. Calvino, C. Lopez, J.A. Perez-Omil and J.M. Rodriguez-Izquierdo, J. Chem. Soc. Faraday Trans. 92 (1996) 2799.
[22] F. Solymosi, Catal. Rev. 1 (1967) 233.
[23] G.M. Schwab, Adv. Catal. 27 (1978) 1.
[24] G.C. Bond, Stud. Surf. Sci. Catal. 11 (1982) 1.
[25] C.C. Kao, S.C. Tsai and Y.W. Chung, J. Catal. 73 (1982) 136.
[26] G.N. Sauvion, J.F. Tempere, M.F. Guilleux, G.D. Mariodassou and D. Delafosse, J. Chem. Soc. Faraday Trans. I 81 (1985) 1357.
[27] J.S. Smith, P.A. Thrower and M.A. Vannice, J. Catal. 68 (1981) 270.
[28] G.C. Bond, in: *Metal–Support and Metal–Additive Effects in Catalysis*, eds. B. Imelik, C. Naccache, G. Coudurier, H. Praliaud, P. Meriaudeau, P. Gallezot, G.A. Martin and J.C. Vedrine (Elsevier, Amsterdam, 1982) p. 1.
[29] V. Ponec, in: *Metal–Support and Metal–Additive Effects in Catalysis*, eds. B. Imelik, C. Naccache, G. Coudurier, H. Praliaud, P. Meriaudeau, P. Gallezot, G.A. Martin and J.C. Vedrine (Elsevier, Amsterdam, 1982) p. 63.
[30] P. Putanov, React. Kinet. Catal. Lett. 35 (1987) 271.
[31] J.M. Campelo, A. Garcia, D. Luna and J.M. Marinas, Appl. Catal. 3 (1982) 315.
[32] J.M. Campelo, A. Garcia, D. Luna and J.M. Marinas, J. Catal. 97 (1986) 108.
[33] F.M. Bautista, J.M. Campelo, A. Garcia, R. Guardeño, D. Luna and J.M. Marinas, J. Chem. Soc. Perkin Trans. II (1989) 493.
[34] F.M. Bautista, J.M. Campelo, A. Garcia, R. Guardeño, D. Luna and J.M. Marinas, J. Catal. 125 (1990) 171.
[35] F.M. Bautista, J.M. Campelo, A. Garcia, R. Guardeño, D. Luna and J.M. Marinas, J. Mol. Catal. 67 (1991) 91.
[36] F.M. Bautista, J.M. Campelo, A. Garcia, R. Guardeño, D. Luna and J.M. Marinas, Stud. Surf. Sci. Catal. 59 (1991) 269.
[37] G. Marcelin, R.F. Vogel and E. Swift, J. Catal. 98 (1986) 64.
[38] G. Marcelin and J.E. Lester, J. Catal. 93 (1985) 270.
[39] S.D. Jacson and L.A. Shaw, React. Kinet. Catal. Lett. 58 (1996) 3.
[40] R. Dhamodharan, Chem. Lett. (1996) 235.
[41] M.A. Aramendia, V. Borau, C. Jimenez, J.M. Marinas, M.E. Sempere and F. Urbano, Appl. Catal. 63 (1990) 375.
[42] M.A. Aramendia, V. Borau, C. Jimenez, J.M. Marinas, M.E. Sempere and F. Urbano, J. Catal. 124 (1990) 286.
[43] C. Minot and P. Gallezot, J. Catal. 123 (1990) 341.
[44] R. Szymanski, H. Charcosset, P. Gallezot, J. Massardier and L. Tournayan, J. Catal. 97 (1986) 366.
[45] D. Poondi and A. Vannice, J. Catal. 161 (1996) 742.
[46] A. Stanislaus and H. Cooper, Catal. Rev. Sci. Eng. 36 (1994) 75.
[47] B. Coughlan and M. Keane, Catal. Lett. 5 (1990) 101.
[48] K. Ohtuka and J. Koga, J. Chem. Lett. (1992) 2073.
[49] Z. Karpin, Adv. Catal. 37 (1990) 45
[50] G. Larsen and G.L. Haller, Catal. Lett. 3 (1989) 103.
[51] V. Ponec, Polyhedron 7 (1988) 2383.
[52] G.A. Somorjai, J. Phys. Chem. 94 (1990) 1013.
[53] G.A. Somorjai, Adv. Catal. 26 (1977) 1.
[54] Z.Z. Lin, T. Okuhara and M. Misono, J. Phys. Chem. 92 (1988) 723.
[55] G.P. Revkevitch, M.K. Mitkova and A.A. Katsnelson, J. Alloys. Comp. 216 (1994) 183.
[56] C.N.J. Wagner and E.N. Aqua, Adv. X-Ray Anal. 7 (1964) 46.
[57] C.A. Pearse and D. Lewis, J. Catal. 26 (1972) 318.
[58] J.I. Langford and A.J.C. Wilson, J. Appl. Cryst. 11 (1978) 102.
[59] L. Hernán, J. Morales and J.L. Tirado, J. Colloid Interface Sci. 110 (1986) 172.
[60] Th.H. de Keijser, J.I. Langford, E.J. Mittemeijer and A.B.P. Vogels, J. Appl. Cryst. 15 (1982) 308.
[61] P.R. Thornton and P.B. Hirsch, Phil. Mag. 3 (1958) 738.
[62] A. Seeger and P. Schiller, Acta Met. 10 (1962) 348.
[63] J.M. Campelo, A. Garcia, D. Luna and J.M. Marinas, Bull. Soc. Chim. Belg. 91 (1982) 131.
[64] J.M. Campelo, A. Garcia, J.M. Gutierrez, D. Luna and J.M. Marinas, Appl. Catal. 7 (1983) 307.
[65] J.M. Campelo, A. Garcia, D. Luna and J.M. Marinas, Bull. Soc. Chim. Belg. 92 (1983) 851.
[66] F.M. Bautista, J.M. Campelo, A. García, R. Guardeño, D. Luna, J.M. Marinas and M.C. Ordoñez, Stud. Surf. Sci. Catal. 78 (1993) 227.
[67] F.M. Bautista, J.M. Campelo, A. García, R. Guardeño, D. Luna and J.M. Marinas, J. Mol. Catal. 104 (1996) 229.
[68] J.M. Campelo, A. García, D. Luna and J.M. Marinas, J. Catal. 111 (1988) 106.
[69] J.M. Campelo, A. García, D. Luna, J.M. Marinas and I. Martinez, Mater. Chem. Phys. 21 (1989) 409.
[70] C. Cativela, J.M. Fraile, J.I. García, J.A. Mayoral, J.M. Campelo, D. Luna and J.M. Marinas, Tetrahedron: Asymmetry 4 (1993) 2507.
[71] F.M. Bautista, J.M. Campelo, A. García, J. León, D. Luna and J.M. Marinas, J. Chem. Soc. Perkin Trans. 2 (1995) 815.
[72] F.M. Bautista, J.M. Campelo, A. García, D. Luna, J.M. Marinas, J.I. García, J.A. Mayoral and E. Pires, Catal. Lett. 36 (1996) 215.
[73] J.M. Campelo, A. Garcia, J.M. Gutierrez, D. Luna and J.M. Marinas, J. Colloid Interface Sci. 95 (1983) 544.
[74] J.M. Campelo, A. Garcia, J.M. Gutierrez, D. Luna and J.M. Marinas, Canad. J. Chem. 61 (1983) 2567.
[75] W.A. Rachinger, J. Sci. Instrum. 25 (1948) 254.
[76] Th.H. de Keijser, E.J. Mittemeijer and H.C.F. Rozendaal, J. Appl. Cryst. 16 (1983) 309.
[77] R.L. Moss, in: *Experimental Methods in Catalytic Research*, Vol. 2, eds. R.B. Anderson and P.T. Dawson (Academic Press, New York, 1976) chapter 2, p. 43.
[78] P. Scherrer, Nachr. Ges. Wiss. Göttingen 26 (1919) 98.
[79] C.N. Satterfield, *Mass Transfer in Heterogeneous Catalysis* (MIT Press, Cambridge, MA, 1970) p. 108.
[80] R. Baltzly, J. Org. Chem. 41 (1976) 920.
[81] Ch.P. Rader and H.A. Smith. J. Am. Chem. Soc. 84 (1962) 1443.
[82] L. Cerveny and V. Ruzicka, Catal. Rev. 24 (1982) 503.
[83] M. Boudart and D. Djega-Mariadassou, *Kinetics of Heterogeneous Catalytic Reactions* (Princeton University Press, Princeton, NJ, 1984) p. 111.
[84] L. Cerveny, P. Skala and V. Ruzicka, J. Mol. Catal. 29 (1985) 33.
[85] L. Cerveny, J. Vopotova and V. Ruzicka, React. Kinet. Catal. Lett. 19 (1982) 223.
[86] L. Cerveny and S. Rehurkova, Collect. Czech. Chem. Commun. 52 (1987) 2909.
[87] J. Barbier, P. Marecot and L. Tifouti, React. Kinet. Catal. Lett. 32 (1986) 269.
[88] R.B. Bartholomew, R.B. Pannel and J.L. Butler, J. Catal. 65 (1980) 335.
[89] C. Moreno-Castilla and F. Carrasco-Marin, J. Chem. Soc. Faraday Trans. 91 (1995) 3519.
[90] M. Boudart and D.J. Sajkowski, Faraday Discuss. 92 (1991) 57.